Multi-Order Stress Intensity Factors Along Three-Dimensional Interface Corners

Tai-Liang Kuo

Chyanbin Hwu

Institute of Aeronautics and Astronautics,
National Cheng Kung University,
Tainan, 70101, Taiwan, R.O.C.

Usually in the study of singularity problems, only the most critical singular order is considered. For three-dimensional interface corner problems, if only the most critical singular order of stresses is considered, it is possible to lose the opportunity to compute the full modes of stress intensity factors. To fully understand the failure behavior of three-dimensional interface corners, a definition of the stress intensity factors for the lower singular orders is proposed in this paper based on that of the most critical singular order. Moreover, to compute the proposed multi-order stress intensity factors accurately and efficiently, a path-independent H-integral, which has been proven useful for the two-dimensional interface corners, is now modified into a domain-independent H-integral for the three-dimensional interface corner problems. Because the stress intensity factors characterize the fracture behavior focused on an arbitrary tip along the corner front, based on anisotropic elasticity the near tip solutions and complementary solutions of two-dimensional generalized plane strain problems are introduced and then utilized for computation of three-dimensional H-integral. To illustrate the validity of the present work, several three-dimensional numerical examples are analyzed and compared with the existing published solutions. Finally, two examples about the interface corners, which occur frequently in electric packages, are solved to show the feasibility and practicability of the proposed approach. [DOI: 10.1115/1.4000411]

Keywords: stress intensity factors, three-dimensional interface corner, domain-independent H-integral

1 Introduction

The evaluation of the stress intensity factors for interface corners is required in many different engineering branches in which the most representative one is electronic packaging. The natural three-dimensional properties (e.g., geometries, loadings, and boundary conditions) cannot be avoided when analyzing a case realistically. Interface corners appearing in most engineering products may be formed by two or more dissimilar media especially in electronic devices (e.g., the corner placed in the solder ball, conductive cooper, and printed wired board shown in the region circled within the dash line of Fig. 1). A commonly used fracture parameter, stress intensity factors (SIFs), is treated as the assessment of the fracture behavior for interface corner in this paper.

Based on the authors' recent studies, it is found that several combinations of interface corners possess more than one singular order of stresses and the most critical one may be associated with one, two, or three modes of stress intensity factors. Therefore, if only the most critical singular order of stress is taken into account, it is possible to lose the opportunity to compute all three modes of stress intensity factors. Recently, Hwu and Kuo [1] presented a unified definition for SIFs of interface corners and cracks. This unified definition is merely correspondent to the most critical singular order of stresses. To deal with the case in which the most critical singular order is not associated with every mode of SIFs, a definition of the SIFs for the lower singular order is proposed in this paper. This extended definition can help us fully understand the failure behavior of interface corners.

In order to compute the SIFs stably and effectively, several different path-independent integrals, such as *J*-integral [2], *L*-integral [3], *M*-integral [4], and *H*-integral [5] were proposed in literature to avoid the complexity of stresses around the crack/corner tip. Because the mixed-mode characteristics and the availability of the near tip and complementary solutions of interface corners, in this paper we adopt the *H*-integral to compute SIFs for three-dimensional interface corners. Even if the *H*-integral was proposed around 35 years ago, most of them were employed to deal with two-dimensional problems such as [6,7] for 2D cracks or corners in homogeneous materials and [1,8–13] for 2D interface cracks or corners between two dissimilar materials. For three-dimensional problems, Meda et al. [14] and Ortiz et al. [15] considered the applications to 3D cracks and solve different modes of stress intensity factors by different *H*-integral. In this paper, a new domain-independent *H*-integral is proposed to deal with all crack/corner problems and all modes of stress intensity factors can be determined simultaneously through one *H*-integral.

When employing *H*-integral to compute the stress intensity factors, the near tip solutions and their associated complementary solutions for the considered crack/corner problems are needed. Although no analytical near tip solutions have been obtained for the general three-dimensional crack/corner problems, in this paper the near tip solutions obtained for the generalized plane stress and generalized plane strain multiwedge problems [16,17] have been proven to be useful for the present 3D crack/corner problems. The reasons for this successful application are (1) along the 3D crack/corner front each point can be treated as a tip of 2D crack/corner, which can be considered to be in generalized plane stress condition for cracks in the outer portion and in generalized plane strain condition for cracks in the inner portion and (2) besides the typical 2D stress/strain components, the additional third directional stress/strain components such as σ_{13}, σ_{23} and ε_{13}, ε_{23} are all available in the solutions obtained by employing Stroh formalism for two-dimensional anisotropic elasticity [18].

Contributed by the Applied Mechanics Division of ASME for publication in the JOURNAL OF APPLIED MECHANICS. Manuscript received June 24, 2008; final manuscript received December 19, 2008; published online March 5, 2010. Assoc. Editor: Zhigang Suo.

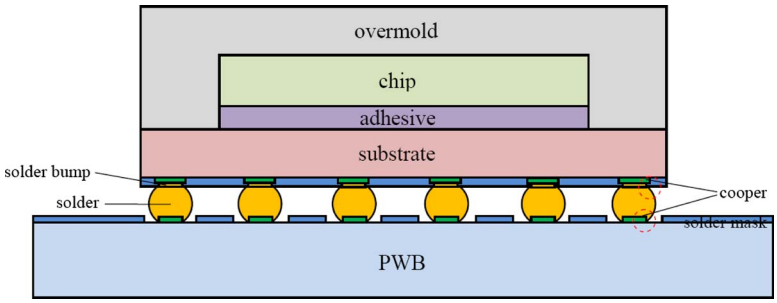

Fig. 1 Possible locations of the interface corners appeared in electronic device

Several benchmark numerical examples, such as an elliptical crack, a through-thickness edge crack, or a through-thickness edge notch in a homogeneous isotropic material subjected to remote tension, and a penny-shaped interface crack between two dissimilar isotropic materials subjected to remote tension, are analyzed for the purpose of comparison. Finally, two examples about the interface corners, which appear frequently in electronic packages, are analyzed to show the feasibility and practicability of the proposed approach.

2 Stress Intensity Factors for the Most Critical Singular Order

If only the most critical singular order of stresses is considered and the possibility of logarithmic singularity is disregarded, by superimposing all the eigenfunctions with the same real part of singular orders, without loss of generality the near tip solutions of two-dimensional interface corners can be expressed as [19]

$$\mathbf{u}(r,\theta) = r^{1-\delta_R}\mathbf{V}(\theta)\langle r^{i\varepsilon_\alpha}\rangle\mathbf{c}, \quad \boldsymbol{\phi}(r,\theta) = r^{1-\delta_R}\boldsymbol{\Lambda}(\theta)\langle r^{i\varepsilon_\alpha}\rangle\mathbf{c} \tag{2.1a}$$

where

$$\mathbf{V}(\theta) = [\boldsymbol{\eta}_1(\theta)\,\boldsymbol{\eta}_2(\theta)\,\boldsymbol{\eta}_3(\theta)], \quad \boldsymbol{\Lambda}(\theta) = [\boldsymbol{\lambda}_1(\theta)\boldsymbol{\lambda}_2(\theta)\boldsymbol{\lambda}_3(\theta)] \tag{2.1b}$$

In the above expressions, (r,θ) is the polar coordinate with origin located on the tip of interface corner; $\mathbf{u}$ and $\boldsymbol{\phi}$ are two 3×1 vectors containing the displacements u_i in x_i-directions and the stress functions ϕ_i, $i=1,2,3$; the angular bracket $\langle\ \rangle$ stands for a diagonal matrix in which each component is varied according to the subscript α, e.g., $\langle z_\alpha\rangle=\text{diag}[z_1,z_2,z_3]$; δ_R and ε_α, $\alpha=1,2,3$ are the real part and imaginary part of the most critical singular orders; $\mathbf{c}$ is a 3×1 coefficient vector; $\boldsymbol{\eta}_\alpha(\theta)$ and $\boldsymbol{\lambda}_\alpha(\theta)$, $\alpha=1,2,3$, are the eigenfunctions associated with $r^{1-\delta_R+i\varepsilon_\alpha}$ whose singular orders are $\delta_R-i\varepsilon_\alpha$. These eigenfunctions are related to the material properties and corner angles of the interface corners, whose detailed expressions can be found in Ref. [1] for multimaterial anisotropic wedges and in Ref. [19] for piezoelectric multiwedges.

Note that in Eq. (2.1), $\mathbf{c}$ is a coefficient vector containing coefficients c_1, c_2, and c_3, which denote the intensities of stresses in the directions of $\boldsymbol{\lambda}_1$, $\boldsymbol{\lambda}_2$, and $\boldsymbol{\lambda}_3$, respectively, and hence are usually treated as the stress intensity factors in literature. However, the directions of $\boldsymbol{\lambda}_1$, $\boldsymbol{\lambda}_2$, and $\boldsymbol{\lambda}_3$ may not be compatible with the directions of interest such as the directions parallel and perpendicular with the crack surface and hence c_1, c_2, and c_3 are sometimes different from the stress intensity factors defined in the conventional fracture mechanics. To build a bridge connecting the failure phenomenon of cracks, interface cracks, corners, and interface corners, a unified definition of stress intensity factor was proposed in our recent study [1] and will be stated later on in Eq. (2.3).

The stress functions ϕ_i are related to the stress components σ_{ij} by

$$\sigma_{i1} = -\phi_{i,2}, \quad \sigma_{i2} = \phi_{i,1} \quad \text{in rectangular coordinate system} \tag{2.2a}$$

or

$$\sigma_{\theta\theta} = \mathbf{n}^T\boldsymbol{\phi}_{,r}, \quad \sigma_{rr} = -\mathbf{s}^T\boldsymbol{\phi}_{,\theta}/r, \quad \sigma_{r\theta} = \mathbf{s}^T\boldsymbol{\phi}_{,r} = -\mathbf{n}^T\boldsymbol{\phi}_{,\theta}/r$$

$$\sigma_{\theta3} = \mathbf{i}_3^T\boldsymbol{\phi}_{,r}, \quad \sigma_{r3} = -\mathbf{i}_3^T\boldsymbol{\phi}_{,\theta}/r \quad \text{in polar coordinate system} \tag{2.2b}$$

where the subscript comma stands for differentiation and the superscript T denotes the transpose of a matrix or a vector and

$$\mathbf{s}^T = (\cos\theta, \sin\theta, 0), \quad \mathbf{n}^T = (-\sin\theta, \cos\theta, 0), \quad \mathbf{i}_3^T = (0,0,1) \tag{2.2c}$$

With the near tip solutions given in Eq. (2.1), a proper definition for the stress intensity factors associated with the most critical singular order has been proposed by Hwu and Kuo [1] as

$$\begin{Bmatrix} K_{\text{II}} \\ K_{\text{I}} \\ K_{\text{III}} \end{Bmatrix} = \lim_{\substack{r\to0 \\ \theta=0}} \sqrt{2\pi}r^{\delta_R}\boldsymbol{\Lambda}\langle(r/\ell)^{-i\varepsilon_\alpha}\rangle\boldsymbol{\Lambda}^{-1}\begin{Bmatrix} \sigma_{r\theta} \\ \sigma_{\theta\theta} \\ \sigma_{3\theta} \end{Bmatrix} \tag{2.3a}$$

or in matrix form

$$\mathbf{k} = \lim_{r\to0}\sqrt{2\pi}r^{\delta_R}\boldsymbol{\Lambda}\langle(r/\ell)^{-i\varepsilon_\alpha}\rangle\boldsymbol{\Lambda}^{-1}\boldsymbol{\phi}_{,r}(r,0) \tag{2.3b}$$

In this definition, ℓ is a reference length used to smooth the physical unit of the stress intensity factors associated with the complex singular orders and the superscript -1 denotes the inverse of a matrix and

$$\boldsymbol{\Lambda} = \boldsymbol{\Lambda}(0) = [\boldsymbol{\lambda}_1\boldsymbol{\lambda}_2\boldsymbol{\lambda}_3] \tag{2.4}$$

The relation between the coefficient vector $\mathbf{c}$ and the stress intensity factor $\mathbf{k}$ is then found to be

$$\mathbf{k} = \sqrt{2\pi}\boldsymbol{\Lambda}\langle(1-\delta_R+i\varepsilon_\alpha)\ell^{i\varepsilon_\alpha}\rangle\mathbf{c} \tag{2.5}$$

Using the relation, Eq. (2.5), the near tip solutions shown in Eq. (2.1) can now be rewritten in terms of the stress intensity factors $\mathbf{k}$ [19]as

$$\mathbf{u}(r,\theta) = \frac{1}{\sqrt{2\pi}}r^{1-\delta_R}\mathbf{V}(\theta)\langle(1-\delta_R+i\varepsilon_\alpha)^{-1}(r/\ell)^{i\varepsilon_\alpha}\rangle\boldsymbol{\Lambda}^{-1}\mathbf{k}$$

$$\boldsymbol{\phi}(r,\theta) = \frac{1}{\sqrt{2\pi}}r^{1-\delta_R}\boldsymbol{\Lambda}(\theta)\langle(1-\delta_R+i\varepsilon_\alpha)^{-1}(r/\ell)^{i\varepsilon_\alpha}\rangle\boldsymbol{\Lambda}^{-1}\mathbf{k} \tag{2.6}$$

By substituting Eq. (2.6) into Eq. (2.2*b*), we can get the near tip stresses in polar coordinate system as

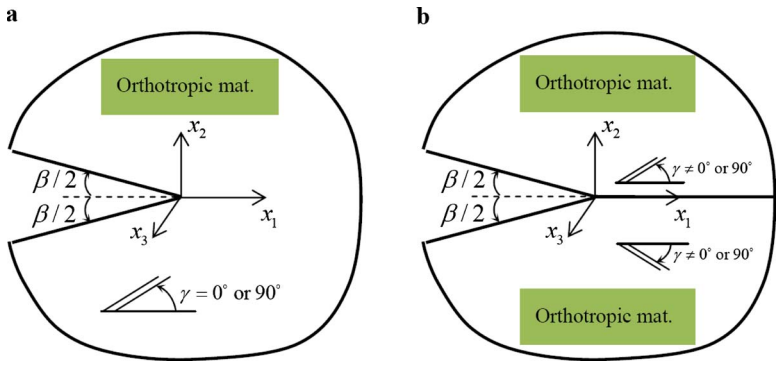

Fig. 2 Special wedges yielding only mode I stress intensity factor: (*a*) a single wedge made up of specially orthotropic materials whose principal material axes are aligned with the nature body axes and (*b*) a biwedge composed of two unidirectional fiber-reinforced composites whose properties are the same but fiber orientations are opposite with respect to x_1-axis

$$\begin{Bmatrix} \sigma_{r\theta} \\ \sigma_{\theta\theta} \\ \sigma_{\theta 3} \end{Bmatrix} = \mathbf{\Omega}(\theta)\boldsymbol{\phi}_{,r}(r,\theta) = \frac{1}{\sqrt{2\pi}} r^{-\delta_R} \mathbf{\Omega}(\theta)\mathbf{\Lambda}(\theta)\langle (r/\ell)^{i\varepsilon_\alpha}\rangle \mathbf{\Lambda}^{-1}\mathbf{k} \tag{2.7a}$$

where

$$\mathbf{\Omega}(\theta) = \begin{bmatrix} \cos\theta & \sin\theta & 0 \\ -\sin\theta & \cos\theta & 0 \\ 0 & 0 & 1 \end{bmatrix} \tag{2.7b}$$

Note that the near tip solutions shown above are not only valid for the interface corners between two dissimilar anisotropic materials but also valid for those among with more than two materials. The most critical singular order may be one real simple root, one real double root with two independent eigenfunctions, one real triple root with three independent eigenfunctions, a pair of complex conjugate roots, or a combination of one real simple root and a pair of complex conjugate roots, etc., [1]. In other words, there are some cases where only one or two coefficients exist for the most critical singular order δ. For example, $c_1 \neq 0$, $\varepsilon_1 = 0$, $c_2 = c_3 = 0$ if δ is a real and simple root; $c_1, c_2 \neq 0$, $\varepsilon_1 = \varepsilon_2 = 0$, $c_3 = 0$ if δ is a real and double root; and $c_2 = \bar{c}_1$, $\varepsilon_2 = -\varepsilon_1$, $c_3 = 0$ if δ is a complex and simple root. In these cases, the missing eigenfunctions can be selected to be the one orthogonal with the existing one or simply taken to be zero. If they are taken to be zero, some of the matrices composed of them such as $\mathbf{V}(\theta)$ and $\mathbf{\Lambda}(\theta)$ will contain one or two zero columns and become singular and hence their inverse will not exist in the common mathematical operation. With this understanding, if the inversion of such matrix is required, inverse it only in its submatrix to avoid the problem of missing eigenfunctions. For example,

$$\begin{bmatrix} a & 0 & 0 \\ 0 & 0 & 0 \\ 0 & 0 & 0 \end{bmatrix}^{-1} = \begin{bmatrix} a^{-1} & 0 & 0 \\ 0 & 0 & 0 \\ 0 & 0 & 0 \end{bmatrix}, \quad \begin{bmatrix} a & b & 0 \\ c & d & 0 \\ 0 & 0 & 0 \end{bmatrix}^{-1} = \frac{1}{\Delta}\begin{bmatrix} d & -b & 0 \\ -c & a & 0 \\ 0 & 0 & 0 \end{bmatrix}, \quad \Delta = ad - bc, \ldots, \text{etc.}$$

Furthermore, sometimes it is not necessary to perform the inversion if the matrix can be multiplied by its own inverse, e.g., $\mathbf{\Lambda}\langle (r/\ell)^{-i\varepsilon_\alpha}\rangle \mathbf{\Lambda}^{-1} = \mathbf{I}$ when $\varepsilon_1 = \varepsilon_2 = \varepsilon_3 = 0$.

Based on the definition given in Eq. (2.3) and the explanation of the inverse operation, it is found that several combinations of interface corners will not possess full modes of stress intensity factors. The following are some examples, which have only one or two modes of stress intensity factors.

Example 1. Special wedges yielding only mode I stress intensity factor.

Since it is difficult to prove analytically which kind of wedge combinations will yield only one or two modes stress intensity factors for the most critical singular order, the observation is made through several different numerical calculations. When a single wedge is made up of *specially orthotropic materials* whose principal material axes are aligned with the nature body axes of the problem such as Fig. 2(*a*) with $\gamma = 0$ deg or 90 deg and $\beta \neq 0$ deg, it is found that many zero components occur in the matrix $\mathbf{\Lambda}$, which will lead two stress functions at $\theta = 0$ and two stress intensity factors vanish. Their detailed zeros are as follows:

$$\mathbf{\Lambda} = \mathbf{\Lambda}(0) = \begin{bmatrix} 0 & 0 & 0 \\ * & 0 & 0 \\ 0 & 0 & 0 \end{bmatrix}, \quad \boldsymbol{\phi}(r,0) = \begin{Bmatrix} 0 \\ * \\ 0 \end{Bmatrix}, \quad k = \begin{Bmatrix} 0 \\ * \\ 0 \end{Bmatrix} \tag{2.8}$$

in which the symbol $*$ denotes nonzero values.

The same situation as that of Eq. (2.8) occurs for a biwedge composed of two unidirectional fiber-reinforced composites whose properties are the same but the fiber orientations are opposite with respect to x_1-axis such as that shown in Fig. 2(*b*) with $\beta \neq 0$ deg. The most critical singular order δ of each case discussed in this example is a real simple root and the inversion of $\mathbf{\Lambda}$ in Eq. (2.8) is not necessary to be performed.

Example 2. Special wedges yielding only modes I and II stress intensity factors.

When a single wedge is made up of *generally orthotropic materials* whose principal material axes are *not* aligned with the nature body axes of the problem such as Fig. 3(*a*) with $\gamma \neq 0$ deg or 90 deg and $\beta \neq 0$ deg or a biwedge composed of two dissimilar orthotropic materials such as Fig. 3(*b*) and 3(*c*) with $\beta \neq 0$ deg, their most critical singular order δ may be a real simple root or two simple complex conjugate roots. Hence

$$\mathbf{\Lambda} = \mathbf{\Lambda}(0) = \begin{bmatrix} * & 0 & 0 \\ * & 0 & 0 \\ 0 & 0 & 0 \end{bmatrix}, \text{ if } \delta \text{ is a real simple root}$$

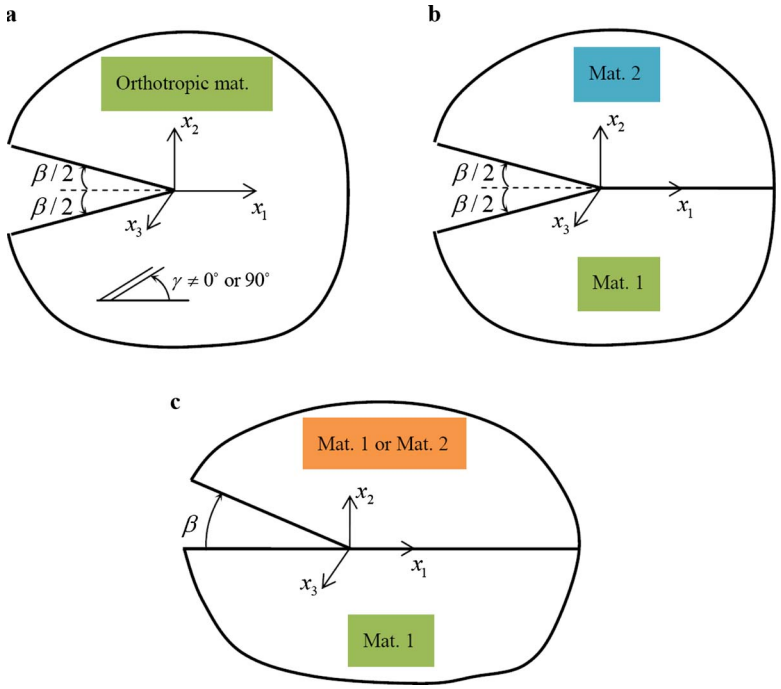

Fig. 3 Special wedges yielding only modes I and II stress intensity factors: (*a*) a single wedge made up of generally orthotropic materials whose principal material axes are not aligned with the nature body axes, (*b*) a biwedge composed of two dissimilar orthotropic materials, and (*c*) a biwedge composed of two dissimilar shaped wedges

$$\mathbf{\Lambda} = \mathbf{\Lambda}(0) = \begin{bmatrix} * & * & 0 \\ * & * & 0 \\ 0 & 0 & 0 \end{bmatrix} \quad \text{if } \delta \text{ are two complex conjugate roots} \tag{2.9a}$$

and their $\boldsymbol{\phi}(r,0)$ and $\mathbf{k}$ will become

$$\boldsymbol{\phi}(r,0) = \begin{Bmatrix} * \\ * \\ 0 \end{Bmatrix}, \quad \mathbf{k} = \begin{Bmatrix} * \\ * \\ 0 \end{Bmatrix} \tag{2.9b}$$

Therefore, for the present example mode III stress intensity factor will be lost when we merely concern the most critical singular order. It should be mentioned that the inversion of $\mathbf{\Lambda}$ in Eq. (2.9*a*) is not necessary to be performed when δ is a real simple root.

3 Stress Intensity Factors for the Lower Singular Orders

From the examples shown in Sec. 2, we see that if only the most critical singular order of stresses is considered, certain modes of stress intensity factors will vanish. However in practical applications, the lost of certain modes of stress intensity factors does not mean that it will not fracture by that mode since the stresses associated with the next critical singular order may dominate the failure behavior. With this understanding, sometimes it is necessary to compute the stress intensity factors for the lower singular orders. To provide a proper definition for the stress intensity factors associated with the lower singular orders, the near tip solutions shown in Eq. (2.6) should be extended to include all the possible singular orders, i.e.,

$$\mathbf{u}(r,\theta) = \mathbf{u}_1(r,\theta) + \mathbf{u}_2(r,\theta) + \mathbf{u}_3(r,\theta) + \cdots$$

$$\boldsymbol{\phi}(r,\theta) = \boldsymbol{\phi}_1(r,\theta) + \boldsymbol{\phi}_2(r,\theta) + \boldsymbol{\phi}_3(r,\theta) + \cdots \tag{3.1}$$

where $\mathbf{u}_1$ and $\boldsymbol{\phi}_1$ are the displacement and stress function vectors associated with the most critical singular order, which are shown in Eq. (2.1) or Eq. (2.6), and $\mathbf{u}_2$, $\boldsymbol{\phi}_2$ and $\mathbf{u}_3$, $\boldsymbol{\phi}_3$ are the displacement and stress function vectors associated with the next two critical singular orders, which may be expressed as

$$\mathbf{u}_j(r,\theta) = \frac{1}{\sqrt{2\pi}} r^{1-\delta_R^{(j)}} \mathbf{V}_j(\theta) \langle (1-\delta_R^{(j)} + i\varepsilon_\alpha^{(j)})^{-1} (r/\ell)^{i\varepsilon_\alpha^{(j)}} \rangle \mathbf{\Lambda}_j^{-1} \mathbf{k}_j$$

$$\boldsymbol{\phi}_j(r,\theta) = \frac{1}{\sqrt{2\pi}} r^{1-\delta_R^{(j)}} \mathbf{\Lambda}_j(\theta) \langle (1-\delta_R^{(j)} + i\varepsilon_\alpha^{(j)})^{-1} (r/\ell)^{i\varepsilon_\alpha^{(j)}} \rangle \mathbf{\Lambda}_j^{-1} \mathbf{k}_j,$$

$$j = 2,3,\ldots \tag{3.2}$$

The subscript j or the superscript (j) denotes the value associated with the jth critical singular order. By the way, similar to $\mathbf{k}$, the stress intensity factors $\mathbf{k}_j$, $j=2,3,\ldots$ associated with the jth critical singular order can be defined as

$$\mathbf{k}_j = \lim_{r\to 0} \sqrt{2\pi} r^{\delta_R^{(j)}} \mathbf{\Lambda}_j \langle (r/\ell)^{-i\varepsilon_\alpha^{(j)}} \rangle \mathbf{\Lambda}_j^{-1} \left[\boldsymbol{\phi}_{,r}(r,0) - \sum_{i=1}^{j-1} \boldsymbol{\phi}_{i,r}(r,0) \right],$$

$$j = 2,3,\ldots \tag{3.3}$$

4 Domain-Independent *H*-Integral for 3D Interface Corners

The same as the 2D interface corner problems in order to avoid the singular and possibly oscillatory behaviors of near corner tip stresses, the most appropriate approach to calculate the stress intensity factors proposed in Eqs. (2.3) and (3.3) is via the path-independent integral. In our recent work [1], we derived a path-independent *H*-integral to compute the stress intensity factors for

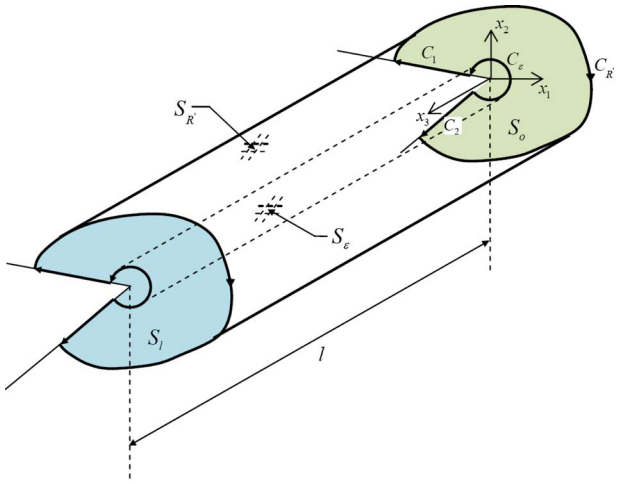

$S = S_o + S_c + S_l$: a closed surface contour

$S_c = S_\varepsilon + S_1 + S_{R'} + S_2$

$C_R = -C_{R'}$: in a counterclockwise direction

Fig. 4 Representative cornered body and illustrations of the constitutive surface and contours

2D interface corner problems. Here, we like to extend our work to derive a three-dimensional version of *H*-integral to deal with 3D interface corner problems.

In the absence of body forces, the reciprocal theorem of Betti and Rayleigh [20] can be expressed as

$$\int_S (\hat{\sigma}_{ij}u_i - \sigma_{ij}\hat{u}_i)n_j dS = 0, \quad i,j = 1,2,3 \tag{4.1}$$

where n_j is the surface normal, σ_{ij} and u_i are the stresses and displacements of the actual system, respectively, while $\hat{\sigma}_{ij}$ and $\hat{u}_i$ are those of the complementary system. S is any closed surface contour surrounding the corner front, which is selected to be $S = S_o + S_c + S_l$ (Fig. 4). S_o is a region on the plane $x_3 = 0$ bounded by C_ε, C_1, C_2, and $C_{R'}$ with an outward unit normal vector $\mathbf{n} = (0,0,-1)$; S_l is a region on the plane $x_3 = l$ bounded by the contours similar to C_ε, C_1, C_2, and $C_{R'}$ with an outward unit normal vector $\mathbf{n} = (0,0,1)$; $S_c = S_\varepsilon + S_1 + S_{R'} + S_2$ in which S_ε, $S_{R'}$, S_1, and S_2 are, respectively, curved boundary surfaces extended by C_ε, $C_{R'}$, C_1, and C_2 from $x_3 = 0$ to $x_3 = l$. If we reverse the integration direction of $S_{R'}$ and denote it by S_R to conform with that of S_ε, i.e., both of these two surface integrals are integrated from $x_3 = 0$ to $x_3 = l$ and from the lower flank ($\theta = \theta_0$) to the upper flank ($\theta = \theta_n$), the outward unit normal vectors of S_R and S_ε will then be denoted by $(n_1, n_2, 0)$ and $(-n_1, -n_2, 0)$.

With $S = S_o + S_c + S_l$, $S_c = S_\varepsilon + S_1 + S_R + S_2$, the normal directions stated above and the traction-free condition on surfaces S_1 and S_2, Eq. (4.1) can now lead to

$$\int_{S_\varepsilon} (\hat{\sigma}_{ij}u_i - \sigma_{ij}\hat{u}_i)n_j dS = \int_{S_R} (\hat{\sigma}_{ij}u_i - \sigma_{ij}\hat{u}_i)n_j dS + \int_{S_l - S_o} (\hat{\sigma}_{i3}u_i - \sigma_{i3}\hat{u}_i) dS \tag{4.2}$$

Replacing dS by ldC for S_ε and S_R, dividing l on both sides of Eq. (4.2) and taking limit of l to zero, we get

$$\int_{C_\varepsilon} (\hat{\sigma}_{ij}u_i - \sigma_{ij}\hat{u}_i)n_j dC = \int_{C_R} (\hat{\sigma}_{ij}u_i - \sigma_{ij}\hat{u}_i)n_j dC + \int_{S_o} (\hat{\sigma}_{i3,3}u_i + \hat{\sigma}_{i3}u_{i,3} - \sigma_{i3,3}\hat{u}_i - \sigma_{i3}\hat{u}_{i,3}) dS \tag{4.3}$$

With the relations $S_o = S_o^R - S_o^\varepsilon$ and $\sigma_{ij}n_j = t_i$ in which t_i stands for surface traction, Eq. (4.3) can be rewritten as

$$\int_{C_\varepsilon} (u_i\hat{t}_i - \hat{u}_i t_i) dC + \int_{S_o^\varepsilon} (\hat{\sigma}_{i3,3}u_i + \hat{\sigma}_{i3}u_{i,3} - \sigma_{i3,3}\hat{u}_i - \sigma_{i3}\hat{u}_{i,3}) dS = \int_{C_R} (u_i\hat{t}_i - \hat{u}_i t_i) dC + \int_{S_o^R} (\hat{\sigma}_{i3,3}u_i + \hat{\sigma}_{i3}u_{i,3} - \sigma_{i3,3}\hat{u}_i - \sigma_{i3}\hat{u}_{i,3}) dS \tag{4.4}$$

which means that the following *H*-integral is domain-independent

$$H = \int_\Gamma (\mathbf{u}^T\hat{\mathbf{t}} - \hat{\mathbf{u}}^T\mathbf{t}) dC + \int_{S_\Gamma} (\hat{\sigma}_{i3,3}u_i + \hat{\sigma}_{i3}u_{i,3} - \sigma_{i3,3}\hat{u}_i - \sigma_{i3}\hat{u}_{i,3}) dS \tag{4.5}$$

In Eq. (4.5), Γ is the path emanating from θ_0 and terminating on θ_n in counterclockwise direction and S_Γ is the region enclosed by the path Γ and the two free edges of interface corners. Equation (4.5) is the three-dimensional version of *H*-integral for interface corner problems. Although similar formula of Eq. (4.5) has been derived in literature [14], their *H*-integral was decoupled into three expressions according to the mode of the employed complementary solutions and was applied to the crack problems only. Here, the domain-independent *H*-integral, Eq. (4.5), can be applied to any crack/corner and interface crack/corner problems and to solve any mode of stress intensity factors with the near tip solution given in Eq. (2.1) or Eq. (2.6) or in Eqs. (3.1) and (3.2).

In order to use the domain-independent property of *H*-integral to calculate the stress intensity factors, like the 2D interface corner problems [1] we first shrink the inner path C_ε into the region dominated by the singular field and make a judicious choice for the integral path (a circular counterclockwise path) and the complementary solution (a near tip solution associated with the singular order $-(1 - \delta_R + i\varepsilon_\alpha)$). Along the circular path, the traction $\mathbf{t} = \boldsymbol{\phi}_{,\theta}/r$, $dC = rd\theta$, and $dS = rd\theta dr$ so Eq. (4.5) becomes

$$H = \int_{\theta_0}^{\theta_n} (\mathbf{u}^T\hat{\boldsymbol{\phi}}_{,\theta} - \hat{\mathbf{u}}^T\boldsymbol{\phi}_{,\theta}) d\theta + \int_0^r \int_{\theta_0}^{\theta_n} (\hat{\sigma}_{i3,3}u_i + \hat{\sigma}_{i3}u_{i,3} - \sigma_{i3,3}\hat{u}_i - \sigma_{i3}\hat{u}_{i,3}) r d\theta dr \tag{4.6}$$

By substituting the near tip solution, Eq. (2.1), and its associated complementary solution into Eq. (4.6), we get

$$H = \hat{\mathbf{c}}^T\mathbf{H}^*\mathbf{c} \tag{4.7a}$$

where

$$\mathbf{H}^* = \int_{\theta_0}^{\theta_n} [\hat{\boldsymbol{\Lambda}}'^T(\theta)\mathbf{V}(\theta) - \hat{\mathbf{V}}^T(\theta)\boldsymbol{\Lambda}'(\theta)] d\theta \tag{4.7b}$$

Note that in Eq. (4.7) no contribution from the second term of Eq. (4.6) has been made since the near tip solution and its associated complementary solution employed in Eq. (4.6) are those for two-dimensional problems whose differentiation with respect to x_3 is equal to zero. Moreover, the terms related to the complex singular orders such as $\langle r^{-i\varepsilon_\alpha} \rangle$ and $\langle r^{i\varepsilon_\alpha} \rangle$ premultiplying and postmultiply-

Table 1 Types of singular orders and stress intensity factors

	Singular orders of stresses			
	δ	Type	SIF	Crack/corner
Ex. 1, Ex. 2	$\delta_1=0.5$	Triple root	K_{I}, K_{II}, K_{III}	Crack
Ex. 3	$\delta_1=0.4555$	Simple root	K_{I}	Notch
	$\delta_2=0.3333$	Simple root	K_{III}	
	$\delta_3=0.0915$	Simple root	K_{II}	
Ex. 4	$\delta_1=0.5\pm0.0855i$	One pair of complex roots and one real root	K_{I}, K_{II}	Interface crack
	$\delta_1=0.5$		K_{III}	
Ex. 5	$\delta_1=0.4667\pm0.0367i$	One pair of complex roots	K_{I}, K_{II}	Interface corner
	$\delta_2=0.4394$	Simple root	K_{III}	
Ex. 6	$\delta_1=0.4946$	Simple root	K_{I}, K_{II}	Interface corner
	$\delta_2=0.3741$	Simple root	K_{III}	

Note: K_{I}, K_{II}, and K_{III} correspond to the opening, shearing, and tearing failure modes, respectively.

ing $\mathbf{H}^*$ are deleted since $\mathbf{H}^*$ is a diagonal matrix in those cases (detailed discussions for five different cases have been provided in Ref. [1]).

If H_i, $i=1,2,3$ denote the value of H with $\hat{c}_i=1$ and $\hat{c}_j=0$, $j\neq i$, a system of simultaneous algebraic equations with unknown c_i, $i=1,2,3$ can be constructed from Eq. (4.7*a*) and be solved as

$$\mathbf{c}=\mathbf{H}^{*-1}\mathbf{h} \tag{4.8a}$$

where

$$\mathbf{h}=\begin{Bmatrix} H_1 \\ H_2 \\ H_3 \end{Bmatrix} \tag{4.8b}$$

By substituting Eq. (4.8) into Eq. (2.5), a direct relation between the stress intensity factors $\mathbf{k}$ and the H-integral $\mathbf{h}$ is obtained as

$$\mathbf{k}=\sqrt{2\pi}\boldsymbol{\Lambda}\langle(1-\delta_R+i\varepsilon_\alpha)\ell^{i\varepsilon_\alpha}\rangle\mathbf{H}^{*-1}\mathbf{h} \tag{4.9}$$

Note that Eqs. (4.8) and (4.9) are general expressions for the computation of the stress intensity factors concerning the most critical singular order in which the singular order can be distinct or repeated, real or complex. The component H_{ij}^* of $\mathbf{H}^*$ is calculated through Eq. (4.7*b*), which can be proven as follows:

Case 1. When the most critical singular order is a real simple root

$$H_{11}^*\neq 0 \quad \text{all other} \quad H_{ij}^*=0$$

Case 2. When the most critical singular order is a real double root

$$H_{ij}^*\neq 0, \quad j=1,2 \quad \text{in general}; \quad H_{3j}^*=H_{j3}^*=0, \quad j=1,2,3$$

Case 3. When the most critical singular order is a real triple root

$$H_{ij}^*\neq 0, \quad j=1,2,3 \quad \text{in general} \tag{4.10}$$

Case 4. When the most critical singular order is a pair of complex root

$$H_{11}^*,H_{22}^*\neq 0 \quad \text{all other} \quad H_{ij}^*=0$$

Case 5. When the most critical singular order is a combination of one real simple root and one pair of complex root

$$H_{11}^*,H_{22}^*,H_{33}^*\neq 0 \quad \text{all other} \quad H_{ij}^*=0$$

From Eq. (4.7*b*), we see that components H_{ij}^* of $\mathbf{H}^*$ are calculated through the two-dimensional near tip solutions provided in Eq. (2.1) or Eq. (2.6), whereas through the domain-independent property proven in Eq. (4.4) the components H_i of $\mathbf{h}$ can be calculated from the 3D version of H-integral defined in Eq. (4.5) through any convenient path Γ emanating from θ_0 and terminating on θ_n in counterclockwise direction. When calculating H_i through Eq. (4.5), $\mathbf{u}$ and $\mathbf{t}$ of the actual 3D state can be obtained from any other methods, while $\hat{\mathbf{u}}$ and $\hat{\mathbf{t}}$ of the virtual state is from the 2D complementary solution with $\hat{c}_i=1$ and $\hat{c}_j=0$, $j\neq i$.

Relation (4.9) tells us that the stress intensity factors $\mathbf{k}$ is influenced locally by $\boldsymbol{\Lambda}$ and $\mathbf{H}^*$ and globally by $\mathbf{h}$. In other words, the corner angles and material properties of the interface corners, which influence the singular orders, will affect the stress intensity factors $\mathbf{k}$ locally through $\boldsymbol{\Lambda}$ and $\mathbf{H}^*$, whereas the effects of external loads or structural geometry will be reflected through $\mathbf{h}$. For example, for a center crack or edge crack in homogeneous materials, their $\boldsymbol{\Lambda}$ and $\mathbf{H}^*$ are the same since their local environments are the same, while their $\mathbf{h}$ is different because their external geometries are different.

Similar to the stress intensity factors for the most critical singular order, the stress intensity factors for the lower singular orders defined in Eq. (3.3) can also be calculated through the domain-independent H-integral derived in Eq. (4.5) and their relations are

$$\mathbf{k}_j=\sqrt{2\pi}\boldsymbol{\Lambda}_j\langle(1-\delta_R^{(j)}+i\varepsilon_\alpha^{(j)})\ell^{i\varepsilon_\alpha^{(j)}}\rangle\mathbf{H}_j^{*-1}\mathbf{h}_j \tag{4.11a}$$

where

$$\mathbf{H}_j^*=\int_{\theta_0}^{\theta_n}[\hat{\boldsymbol{\Lambda}}_j'^T(\theta)\mathbf{V}_j(\theta)-\hat{\mathbf{V}}_j^T(\theta)\boldsymbol{\Lambda}_j'(\theta)]d\theta \quad \text{no summation on } j \tag{4.11b}$$

5 Numerical Examples

For the interface corners, the near tip solutions which consider the most critical singular order of stresses and all the lower singular orders are provided in Eqs. (2.1) and (3.1), while a three-dimensional version of the domain-independent H-integral is derived in Eq. (4.5). To calculate the stress intensity factors defined in Eqs. (2.3) and (3.3), a direct relation between the stress intensity factors and the H-integral has been obtained in Eqs. (4.9) and (4.11). To illustrate the accuracy and versatility of the present work for 3D interface corner problems, several numerical examples are shown in this section such as (i) an elliptical central crack in a homogeneous isotropic material subjected to remote tension, (ii) a through-thickness edge crack in a homogeneous isotropic material subjected to remote tension, (iii) a through-thickness edge notch in a homogeneous isotropic material subjected to remote tension, (iv) a penny-shaped interface crack between two dissimilar isotropic materials subjected to remote tension, (v) a through-thickness interface corner between two dissimilar materials subjected to remote tension, and (vi) a representative block of electronic package subjected to tensile loading. The singular orders and their associated modes of SIF are sorted in Table 1 for these crack/notch/interface crack/interface corner problems. Although in this table, all the examples contain full modes of stress intensity factors K_{I}, K_{II}, and K_{III} by including the lower singular orders δ_2 and/or δ_3, it should be noted that in our

numerical experiments there are still some cases of notches and interface corners which have only two distinct real simple roots associated with only two modes of stress intensity factors.

In the following examples, to calculate **k** through Eq. (4.9) or Eq. (4.11), the stresses and displacements of the actual system needed in calculating H_i of **h** from Eq. (4.5) are obtained from the commercial finite element software ANSYS. For convenience, the integral domain is chosen to be a surface bounded by a circular path emanating from the lower crack/corner surface and terminating on the upper crack/corner surface, and the normal of this integral surface domain is tangent to the crack front. Moreover, the surface integral is performed through a two-stage numerical line integral (e.g., trapezoidal method or Simpson's method) with respect to θ and r one by one, i.e., $dS=rd\theta dr$. The two-stage line integral means that we perform the integral firstly with respect to θ and we can get several results which are scalar functions of r; then we proceed to integrate with respect to r and consequently the surface integral is complete. Because the circular domain is employed, the integration paths with respect to θ are also selected to be circular and pass through nodal points in our examples. Since the numerical output will depend on element meshes and integration paths, the convergent test and domain-independent study were done numerically before performing all the following examples. It should be mentioned that although the domain-independent property of H-integral has been proven theoretically in Sec. 4, when using H-integral to calculate the stress intensity factors we still have to avoid taking the numerical results overly close to the corner tip because of the incorrect stress information in the neighborhood of the corner tip provided by finite element analysis.

To avoid the incorrect stress information near the corner/crack tip is the main reason why the path-independent integrals play important roles in the computation of fracture parameters. To show the difficulty of convergence through the conventional approach via the definition of stress intensity factors, an illustration is given in example 5 for the typical interface corner problems.

Example 1. An elliptical central crack in a homogeneous isotropic material subjected to remote tension.

First, we discuss an example about an isotropic cylinder with an elliptical central crack. This example is a conventional 3D crack problem whose singular order is a well known number 0.5, which is a real triple root with three independent eigenfunctions. Through relation (4.9), it can be calculated that

$$\mathbf{k}=\frac{\sqrt{2\pi}}{2}\begin{bmatrix}0 & \lambda_{21} & 0\\ \lambda_{12} & 0 & 0\\ 0 & 0 & \lambda_{33}\end{bmatrix}\begin{bmatrix}H_{11}^{*} & H_{12}^{*} & H_{13}^{*}\\ H_{21}^{*} & H_{22}^{*} & H_{23}^{*}\\ H_{31}^{*} & H_{32}^{*} & H_{33}^{*}\end{bmatrix}^{-1}\begin{Bmatrix}H_1\\ H_2\\ H_3\end{Bmatrix}=\begin{Bmatrix}K_{\mathrm{II}}\\ K_{\mathrm{I}}\\ K_{\mathrm{III}}\end{Bmatrix} \tag{5.1}$$

which shows that *in general*, no mode of the stress intensity factors will be lost if only the most critical singular order is considered, and hence it is not necessary to consider the stress intensity factors for the lower singular orders. In Eq. (5.1), λ_{ij} and H_{ij}^{*} can be calculated through Eqs. (2.4) and (4.7*b*) in which the near tip solutions $\mathbf{\Lambda}(\theta),\mathbf{V}(\theta)$ and their associated complementary solutions $\hat{\mathbf{\Lambda}}(\theta),\hat{\mathbf{V}}(\theta)$ have been provided in Ref. [1]. Whereas H_i is calculated through Eq. (4.5) in which **u**, **t**, and σ_{i3} are the displacement, traction, and stress, respectively, of the actual system. To obtain the data from the actual system and to compare the results with the existing analytical solution derived by Irwin [21], a finite element model of isotropic cylinder with an elliptical central crack was constructed and executed using ANSYS. The numerical results of stress intensity factors calculated this way proved the property of domain-independency and the accuracy of the present method since the maximum relative error is below 0.5%, which is acceptable. (To save the space of this paper, the numerical results are not shown here.)

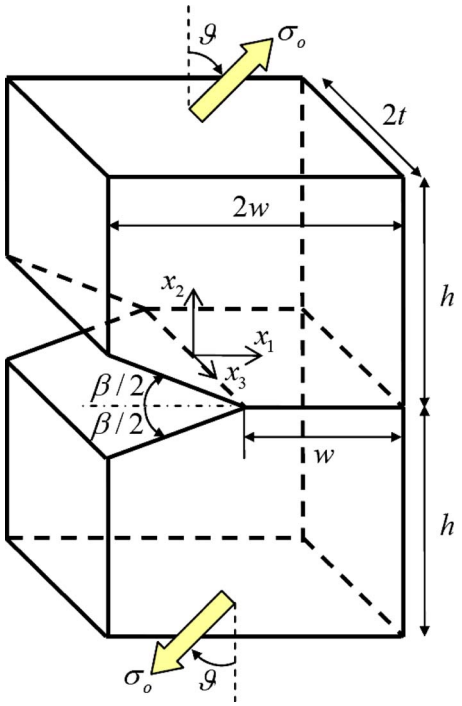

Fig. 5 A through-thickness edge notch in a homogeneous isotropic material subjected to remote tension

Example 2. A through-thickness edge crack in a homogeneous isotropic material subjected to remote tension.

Consider an isotropic rectangular parallelepiped with a through-thickness edge crack under remote tension. Since the local environments of the edge crack and center crack are the same, the relation for the previous example, Eq. (5.1), is still valid for the present example. The difference in these two examples comes from the external environments, which will be reflected through the vector **h** containing the values of H-integral H_1, H_2, and H_3. With this understanding, a numerical example presented by Li et al. [22], Sukumar et al. [23], and Raju and Newmann [24] for edge crack has been done for the purpose of comparison and our results agree with them with difference below 4.03%.

Example 3. A through-thickness edge notch in a homogeneous isotropic material subjected to remote tension.

In order to accentuate that the proposed approach is not only applied to the cracked problems but also suitable for the general corner problems, a through-thickness edge notch in an isotropic specimen under remote tension is considered in this example (Fig. 5). The dimensions of the specimen used in this example are as follows: $w=1$ mm, $h=2w$, $t=0.7w$, and $\beta=90$ deg, which are the half-width, half-height, half-thickness, and notch angle of this specimen. The surfaces at $x_3=\pm t$ are traction-free. The remote tension σ_o is specified as 10 MPa with $\vartheta=0$ deg or $\vartheta=45$ deg. The Young's modulus and Poisson's ratio of this specimen are 210 GPa and 0.3, respectively. For the purpose of comparison, the boundary conditions set in the analysis are as follows: $u_3=0$ on the surface $x_3=0$ and $u_1=u_2=0$ on the line $x_1=w$ and $x_2=0$ to simulate the situation presented by Ortiz et al. [15]. Note that to prevent the rotation of the body induced by the inclined tension σ_o with $\vartheta=45$ deg, the boundary condition $u_1=0$ is set on two lines ($x_1=w$ and $x_2=0.0875w$) and ($x_1=w$ and $x_2=-0.0875w$).

When using the key matrix provided in Refs. [1,16,17] to solve the singular orders for the present example, we obtain three distinct real simple roots, i.e., $\delta=0.4555$, $\delta^{(2)}=0.3333$, and $\delta^{(3)}=0.0915$, where each root is accompanied with only one real eigenfunction. By Eqs. (4.9) and (4.11), we obtain

Table 2 Stress intensity factors (K_I, K_{II}, K_{III}) versus the corner front location x_3 for a through-thickness edge notch in a homogeneous isotropic material subjected to remote tension

	K_I (MPa mm$^{0.4555}$) ($K_{II}^{(1)}=K_{III}^{(1)}=0$)			K_{II} (MPa mm$^{0.0915}$) ($K_I^{(2)}=K_{III}^{(2)}=0$)		K_{III} (MPa mm$^{0.3333}$) ($K_I^{(3)}=K_{II}^{(3)}=0$)	
x_3 (mm)	[15] $\vartheta=0$ deg	Present $\vartheta=0$ deg	Present $\vartheta=45$ deg	Present $\vartheta=0$ deg	Present $\vartheta=45$ deg	Present $\vartheta=0$ deg	Present $\vartheta=45$ deg
0.1	60.7426	61.6524	43.5633	0	−146.1639	0	−1.7789
0.2	60.5156	61.4941	43.4481	0	−146.7951	0	−3.7520
0.3	60.2188	61.2071	43.2694	0	−148.1272	0	−6.1410
0.4	59.8057	60.6773	42.8787	0	−150.3025	0	−9.2417
0.5	58.3217	59.6714	42.1616	0	−153.8029	0	−13.5589
0.6	55.1094	57.2572	40.4526	0	−160.1900	0	−20.1721
Plane strain		58.1937	41.1658	0	−153.3050	0	0

$$\mathbf{k} = 0.5445^*\sqrt{2\pi}\begin{bmatrix}0&0&0\\ \lambda_{12}&0&0\\ 0&0&0\end{bmatrix}\begin{bmatrix}1/H_{11}^*&0&0\\ 0&0&0\\ 0&0&0\end{bmatrix}\begin{Bmatrix}H_1\\H_2\\H_3\end{Bmatrix}=\begin{Bmatrix}0\\K_I\\0\end{Bmatrix}$$

$$\mathbf{k}_2 = 0.6667^*\sqrt{2\pi}\begin{bmatrix}0&0&0\\ 0&0&0\\ \lambda_{13}^{(2)}&0&0\end{bmatrix}\begin{bmatrix}1/H_{11}^{*(2)}&0&0\\ 0&0&0\\ 0&0&0\end{bmatrix}\begin{Bmatrix}H_1^{(2)}\\H_2^{(2)}\\H_3^{(2)}\end{Bmatrix}=\begin{Bmatrix}0\\0\\K_{III}\end{Bmatrix}$$

$$\mathbf{k}_3 = 0.9085^*\sqrt{2\pi}\begin{bmatrix}\lambda_{11}^{(3)}&0&0\\ 0&0&0\\ 0&0&0\end{bmatrix}\begin{bmatrix}1/H_{11}^{*(3)}&0&0\\ 0&0&0\\ 0&0&0\end{bmatrix}\begin{Bmatrix}H_1^{(3)}\\H_2^{(3)}\\H_3^{(3)}\end{Bmatrix}=\begin{Bmatrix}K_{II}\\0\\0\end{Bmatrix} \tag{5.2}$$

in which the superscripts (2) and (3) of λ_{ij}, H_{ij}^*, and H_i denote the values associated with $\delta^{(2)}$ and $\delta^{(3)}$, respectively, while those without the superscript are the values associated with the most critical singular order δ.

From Eq. (5.2), we see that if only the most critical singular order is considered, two modes of the stress intensity factors will be lost and only K_I exists no matter what kind of loads is applied because the external loading conditions will influence the results through **h** only, i.e., H_i, $i=1,2,3$. Table 2 shows the results of K_I, K_{II}, and K_{III} versus x_3 for two different loading conditions with the inclusion of the next two lower singular orders. From this table, we see that the present results agree well with those presented by Ortiz et al. [15] for the case of $\vartheta=0$ deg. While the results for $\vartheta=45$ deg validate the statement that if only the most critical singular order is considered, only K_I exists even for the mixed mode loading condition. That is also the reason we consider the stress intensity factors associated with the lower singular orders in this paper.

Example 4. A penny-shaped interface crack between two dissimilar isotropic materials subjected to remote tension.

In the last three examples, the cracks or corners are considered to be located in the homogeneous materials. To show that the present study can also deal with the interface cracks or corners, we consider a penny-shaped interface crack between two dissimilar isotropic materials subjected to remote tension. The analytical solution of this problem was presented by Kassir and Bregman [25] and Chaudhuri [26] as

$$K_I + iK_{II} = 2\sigma_o\sqrt{a}\frac{\Gamma(2+i\varepsilon)}{\Gamma(0.5+i\varepsilon)} \tag{5.3}$$

where Γ is the Gamma function, ε is the oscillation index, i.e., the imaginary part of the most critical singular order, σ_o is the applied tension on the remote ends or the crack surfaces, and a is the radius of the penny-shaped crack.

Figure 6 is a quarter plot of the cylinder composed of two different materials in which a penny-shaped crack is embedded on the interface between materials 1 and 2. The two materials are both isotropic whose elastic properties are as follows: $E=150$ GPa, $\nu=0.3$ for material 1 and $E=20$ GPa, $\nu=0.25$ for material 2. The radius of the penny-shaped crack, radius of the cylinder cross section, and half height of the cylinder used in this example are $a=0.005$ mm, $b=10a$, and $h=10a$. The applied remote tension σ_o is 10 MPa. The boundary conditions used in finite element analysis are $u_1=0$ on the surface $x_1=0$, $u_3=0$ on the surface $x_3=0$, and $u_2=0$ on the line $\rho=b$ and $x_2=0$. The singular orders of this example are calculated as $0.5\pm0.0855i$ and 0.5 accompanied with one pair of complex conjugate eigenfunctions and one real eigenfunction. Because these three singular orders have the same real part, they are all parts of the most critical singular order and hence Eq. (4.9) can be written as

$$\mathbf{k} = \sqrt{2\pi}\begin{bmatrix}\lambda_{11}&\bar{\lambda}_{11}&0\\ \lambda_{12}&\bar{\lambda}_{12}&0\\ 0&0&\lambda_{33}\end{bmatrix}\times\begin{bmatrix}(0.5+0.0855i)\ell^{0.0855i}&0&0\\ 0&(0.5-0.0855i)\ell^{-0.0855i}&0\\ 0&0&0.5\end{bmatrix}\times\begin{bmatrix}H_{11}^*&0&0\\ 0&\bar{H}_{11}^*&0\\ 0&0&H_{33}^*\end{bmatrix}^{-1}\begin{Bmatrix}H_1\\\bar{H}_1\\H_3\end{Bmatrix}=\begin{Bmatrix}K_{II}\\K_I\\K_{III}\end{Bmatrix} \tag{5.4}$$

in which the reference length ℓ is selected to be 0.01 mm. From Eq. (5.4), we see that no mode will be lost if we merely consider the most critical singular order in this example. For the present pure tension case, $H_1\neq0$ and $H_3=0$.

In addition to the domain-independence proven theoretically in Eq. (4.4), to get further evidence for the domain-independence of H-integral, in this example we choose three different rectangular paths with wide range as shown in Figure 7. Table 3 shows that the stress intensity factors calculated through different paths are almost the same as those calculated by the analytical solution (5.3).

Example 5. A through-thickness interface corner between two dissimilar materials subjected to remote tension.

For the purpose of comparison, the above four examples consider only isotropic materials. To show that the generality of the present study, which is applicable to any kind of anisotropic materials in this example, we consider the 3D interface corner between one isotropic material and one orthotropic material. Figure 8 is a schematic diagram of the present example in which $d=5$ mm, $W/d=3$, $h/W=1/15$, $t/W=2$, $L/W=6.0$, $\alpha=30$ deg, and $\sigma_o=10$ MPa where $x_3=\pm t/2$ are the free surfaces. The material above the interface is isotropic whose elastic properties are $E=10$ GPa, $\nu=0.2$, while the other portion is orthotropic whose

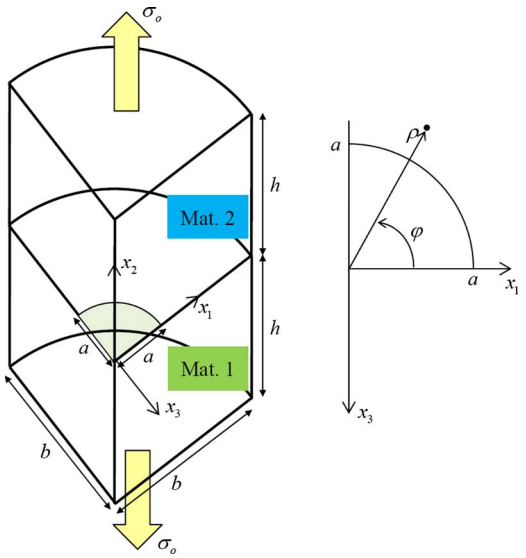

Fig. 6 A penny-shaped interface crack between two dissimilar isotropic materials subjected to remote tension

elastic properties are $E_{11}=134.45$ GPa, $E_{22}=E_{33}=11.03$ GPa, $G_{12}=G_{13}=5.84$ GPa, $G_{23}=2.98$ GPa, $\nu_{12}=\nu_{13}=0.301$, and $\nu_{23}=0.49$. The boundary conditions used in the analysis are $u_1=0$ on the surface $x_1=d$, $u_2=0$ on the surface $x_2=-L/2$, and $u_3=0$ on the surface $x_3=0$. The singular orders of this example are obtained as $0.4667\pm0.0367i$ and 0.4394 accompanied with one pair of complex conjugate eigenfunctions and one real eigenfunction. Because the real part of the complex singular order is higher than the real singular order, $0.4667\pm0.0367i$ will be treated as the most critical singular order. To compute their associated stress intensity factors, we use Eqs. (4.9) and (4.11) which can be shown as

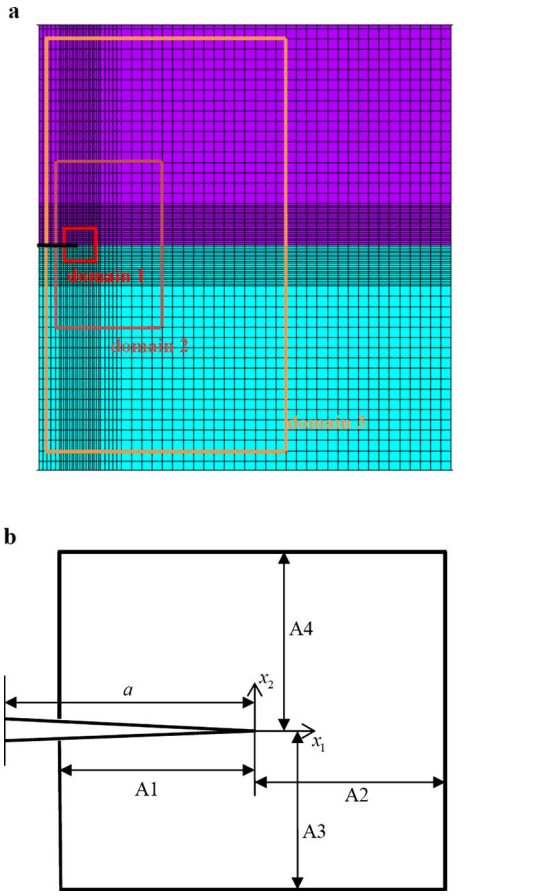

Fig. 7 (*a*) Three rectangular integral domains for a penny-shaped interface crack and (*b*) dimensions of the integral domains

$$\mathbf{k}=\sqrt{2\pi}\begin{bmatrix}\lambda_{11} & \bar{\lambda}_{11} & 0\\ \lambda_{12} & \bar{\lambda}_{12} & 0\\ 0 & 0 & 0\end{bmatrix}\begin{bmatrix}(0.5333+0.0367i)\ell^{0.0367i} & 0 & 0\\ 0 & (0.5333-0.0367i)\ell^{-0.0367i} & 0\\ 0 & 0 & 0\end{bmatrix}\begin{bmatrix}1/H_{11}^{*} & 0 & 0\\ 0 & 1/\bar{H}_{11}^{*} & 0\\ 0 & 0 & 0\end{bmatrix}\begin{Bmatrix}H_1^{(1)}\\ \bar{H}_1^{(1)}\\ H_3^{(1)}\end{Bmatrix}=\begin{Bmatrix}K_{\mathrm{II}}\\ K_{\mathrm{I}}\\ 0\end{Bmatrix}$$

$$\mathbf{k}_2=0.5606^{*}\sqrt{2\pi}\begin{bmatrix}0 & 0 & 0\\ 0 & 0 & 0\\ \lambda_{13}^{(2)} & 0 & 0\end{bmatrix}\begin{bmatrix}1/H_{11}^{*(2)} & 0 & 0\\ 0 & 0 & 0\\ 0 & 0 & 0\end{bmatrix}\begin{Bmatrix}H_1^{(2)}\\ H_2^{(2)}\\ H_3^{(2)}\end{Bmatrix}=\begin{Bmatrix}0\\ 0\\ K_{\mathrm{III}}\end{Bmatrix} \tag{5.5}$$

Table 3 Stress intensity factors of a penny-shaped interface crack

	A1	A2	A3	A4	K_{I} (MPa mm$^{0.5}$)	K_{II} (MPa mm$^{0.5}$)	K_{III} (MPa mm$^{0.5}$)
Path 1	0.4a	0.4a	0.4a	0.4a	0.790268	0.161250	0
Path 2	0.6a	2a	2a	2a	0.793557	0.165903	0
Path 3	0.8a	5a	5a	5a	0.789795	0.167781	0
Eq. (5.3)					0.793788	0.162894	–

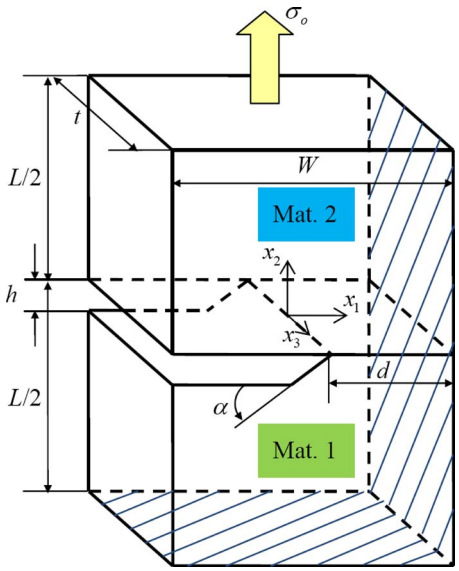

Fig. 8 A through-thickness interface corner between two dissimilar materials subjected to remote tension

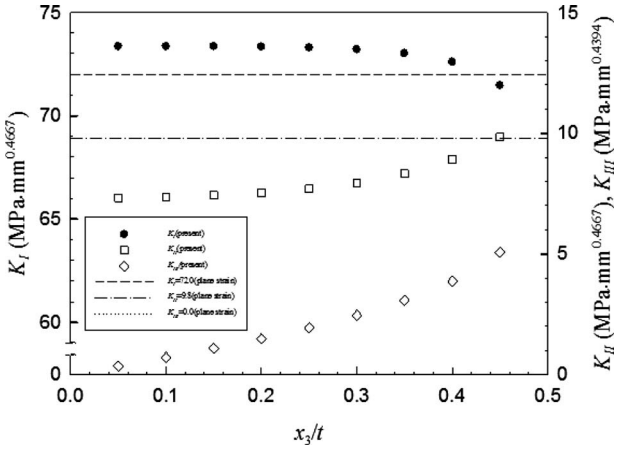

Fig. 9 Stress intensity factors for a through-thickness interface corner between two dissimilar materials subjected to remote tension

in which the reference length ℓ is selected to be 10 mm.

From Eq. (5.5), we see that if only the most critical singular order is considered mode III stress intensity factor will be lost no matter what kind of loading is applied, which will then be picked up by considering the next higher singular order. Figure 9 shows the results of K_I, K_{II}, and K_{III} versus x_3/t for the present example. From this result we see that the stress intensity factors in the inner part of the interface corner will approach to certain constant values not far away from those of the corresponding plane strain problems discussed in Ref. [1], which is acceptable from the engineering viewpoint.

While the advantage of path-independent integrals for crack problems has been shown in the literature for a long time, relatively few examples have been presented for three-dimensional interface corners. Since the domain-independent characteristics of *H*-integral has been proven theoretically in Sec. 4 and numerically in example 4, all the numerical solutions given in this paper are presented without any convergent difficulties. To show the advantage of the present *H*-integral, the following are the results obtained through the conventional approach, i.e., calculated via defi-

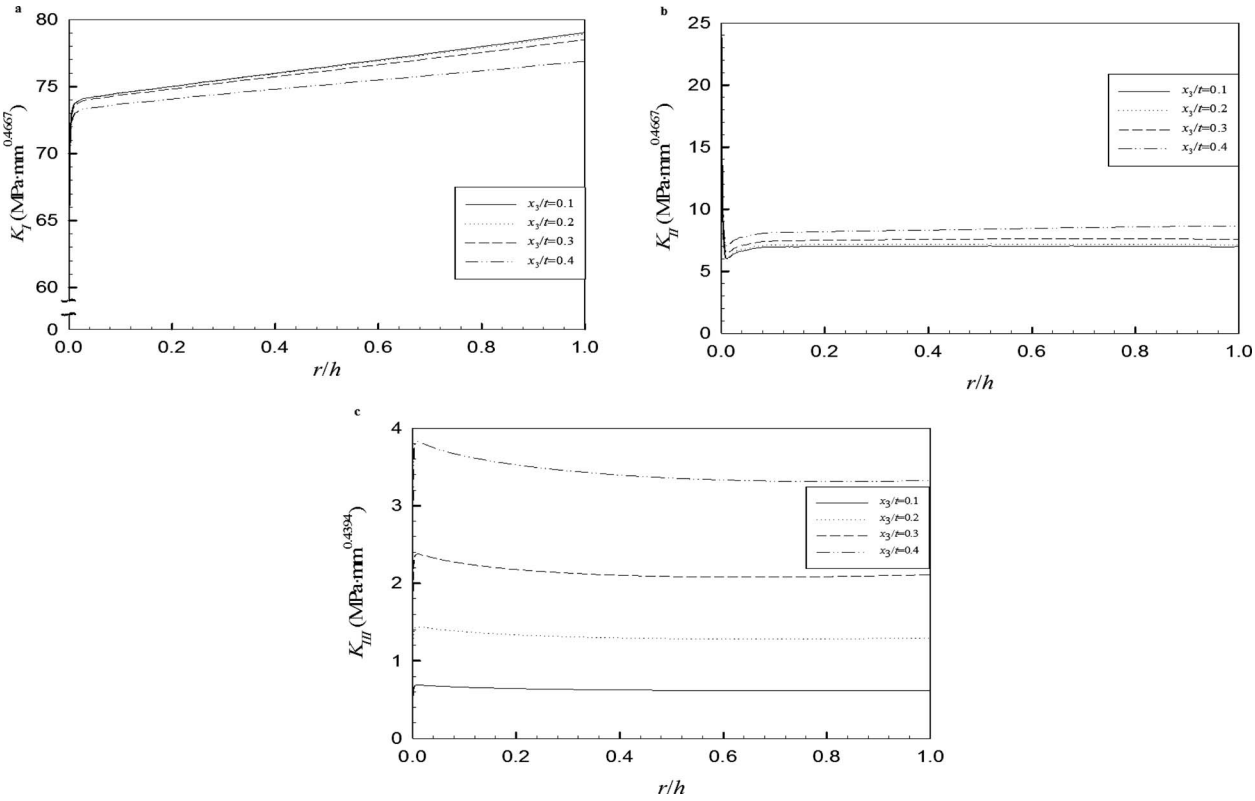

Fig. 10 Stress intensity factors for a through-thickness interface corner calculated directly from the definitions, Eqs. (2.3) and (3.3): (*a*) K_I, (*b*) K_{II}, and (*c*)K_{III}

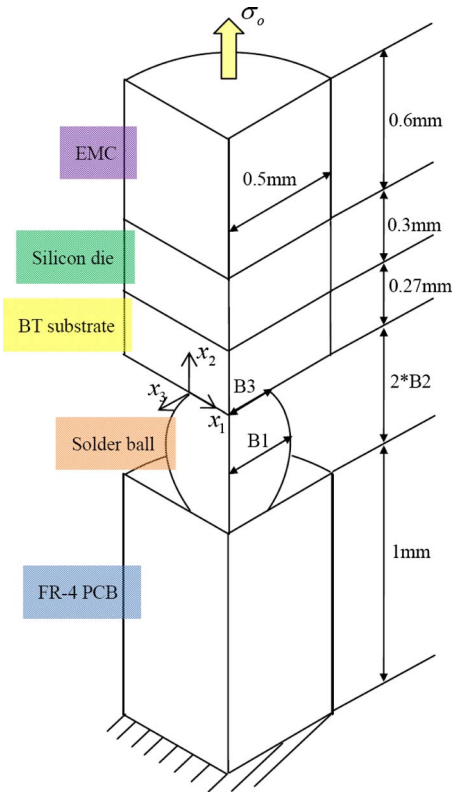

Fig. 11 A representative block of electronic package and the dimensions of each portion

nition (2.3) or (3.3), which will then encounter the convergent difficulty. Figures 10(*a*)–10(*c*) are plots of stress intensity factors K_{I}, K_{II}, and K_{III} versus the distance to the corner tip r/h. From these figures, we see that the values of stress intensity factors become unstable and cannot be convergent to a definite value, and hence it is really difficult to terminate the approaching of r to zero. This problem is due to the complexity and infinity of stresses near the interface corners, which can be avoided in the calculation through H-integral by using the path away from the corner tip.

Example 6. A representative block of electronic package subjected to tensile loading.

For the purpose of giving a good connection between the present method and the real engineering problem, a representative block of electronic package is discussed in this example. Figure 11 is a quarter plot of the representative block in which the interface corner between the solder ball and BT substrate is analyzed to discuss the effect of the radius of solder ball (B1) on the stress intensity factors. The dimensions of each portion are also shown in Fig. 11 in which B2=0.8*B1 and B3=0.6*B1. This discussion is helpful to realize the relevancy between the radius of solder ball and the reliability of electronic package. The boundary and loading conditions are the entire bottom of the block is clamped and the entire top is subjected to $\sigma_o=10$ MPa. The properties of each constitutive material are assumed to be linear elastic and listed in Table 4. The singular orders are obtained as $\delta_1=0.4946$ and $\delta_2=0.3741$, and each one is accompanied with only one real eigenfunction. By using Eqs. (4.9) and (4.11), we get

$$\mathbf{k}=0.5054^{*}\sqrt{2\pi}\begin{bmatrix}\lambda_{11} & 0 & 0\\ \lambda_{12} & 0 & 0\\ 0 & 0 & 0\end{bmatrix}\begin{bmatrix}1/H_{11}^{*} & 0 & 0\\ 0 & 0 & 0\\ 0 & 0 & 0\end{bmatrix}\begin{Bmatrix}H_1\\ H_2\\ H_3\end{Bmatrix}=\begin{Bmatrix}K_{\mathrm{II}}\\ K_{\mathrm{I}}\\ 0\end{Bmatrix}$$

Table 4 Material properties of the representative electronic package block

Materials	Young's modulus (GPa)	Poisson's ratio
EMC	16	0.25
Silicon die	131	0.3
BT substrate	26	0.11
Solder ball	10.375	0.4
FR-4 PCB	22	0.11

$$\mathbf{k}_2=0.6259^{*}\sqrt{2\pi}\begin{bmatrix}0 & 0 & 0\\ 0 & 0 & 0\\ \lambda_{13}^{(2)} & 0 & 0\end{bmatrix}\begin{bmatrix}1/H_{11}^{*(2)} & 0 & 0\\ 0 & 0 & 0\\ 0 & 0 & 0\end{bmatrix}\begin{Bmatrix}H_1^{(2)}\\ H_2^{(2)}\\ H_3^{(2)}\end{Bmatrix}=\begin{Bmatrix}0\\ 0\\ K_{\mathrm{III}}\end{Bmatrix} \tag{5.6}$$

From Eq. (5.6), we see that if only the most critical singular order is considered the mode III stress intensity factor will be lost. The mode III stress intensity factor will be obtained only when the next higher singular order is taken into account. However, the values of K_{III} on the entire crack front are equal to zero because of the axially symmetric properties of this example (i.e., $H_1^{(2)}=0$). Table 5 lists the trends of stress intensity factors versus radii of solder balls from which we see that under the same loading and boundary conditions the stress intensity factors will decrease when the size of solder ball increases.

6 Conclusions

In this paper, the importance of the lower singular orders is illustrated and a newly modified domain-independent H-integral is proposed for three-dimensional interface corner problems. The proposed definition for the multi-order stress intensity factors and the three-dimensional version of H-integral are valid for cracks, interface cracks, corners, and interface corners. The related materials can be any kind of anisotropic materials including the degenerate materials such as the isotropic materials. The most critical singular orders induced by different combinations of interface corners can be a real simple root, a real double root, a real triple root, a pair of complex conjugates, or a real simple root combined with a pair of complex conjugates, etc. Similarly, the lower singular orders can also have any different kinds of combinations. Even several different kinds of combinations are considered in the present paper, all the stress intensity factors can be determined directly through the relation shown in Eq. (4.9). In this simple relation, $\mathbf{\Lambda}$ and $\mathbf{H}^{*}$ are determined through the near tip solution and its associated complementary solution, and hence will reflect the local behavior of the interface corners; whereas $\mathbf{h}$ containing the values of 3D H-integral will then reflect the effects of external loading and structural geometry. Therefore, through the contents of these matrices it is helpful for us to understand the details of multi-order stress intensity factors for the general three-dimensional interface corners. Detailed discussions for several different kinds of problems have been presented in our numerical examples, which show that our proposed approach is not only versatile but also efficient and accurate.

Table 5 Stress intensity factors versus radii of solder ball

	K_{I} (MPa mm$^{0.4946}$)	K_{II} (MPa mm$^{0.4946}$)	K_{III} (MPa mm$^{0.3741}$)
B1=0.30 mm	71.8297	−19.5833	0
B1=0.45 mm	38.5033	−10.4973	0
B1=0.60 mm	24.6453	−6.7192	0
B1=0.75 mm	17.4269	−4.7512	0

Acknowledgment

The authors would like to thank the National Science Council, Taiwan, R.O.C. for support through Grant NSC 95-2221-E-006-144-MY3. T.-L.K. is also grateful to the financial support from the Advanced Semiconductor Engineering (ASE), Inc.

References

[1] Hwu, C., and Kuo, T. L., 2007, "A Unified Definition for Stress Intensity Factors of Interface Corners and Cracks," Int. J. Solids Struct., **44**, pp. 6340–6359.
[2] Rice, J. R., 1968, "A Path Independent Integral and the Approximate Analysis of Strain Concentration by Notches and Cracks," ASME J. Appl. Mech. **35**, pp. 379–386.
[3] Choi, N. Y., and Earmme, Y. Y., 1992, "Evaluation of Stress Intensity Factors in a Circular Arc-Shaped Interfacial Crack Using *L*-Integral," Mech. Mater., **14**, pp. 141–1c53.
[4] Im, S., and Kim, K. S., 2000, "An Application of Two-State *M*-Integral for Computing the Intensity of the Singular Near-Tip Field for a Generic Wedge," J. Mech. Phys. Solids, **48**, pp. 129–151.
[5] Stern, M., 1973, "A Boundary Integral Representation for Stress Intensity Factors," Recent Advances in Engineering Science, **7**, pp. 125–132.
[6] Stern, M., Becker, E. B., and Dunham, R. S., 1976, "A Countour Integral Computation of Mixed-Mode Stress Intensity Factors," Int. J. Fract., **12**(3), pp. 359–368.
[7] Sinclair, G. B., Okajima, M., and Griffin, J. H., 1984, "Path Independent Integrals for Computing Stress Intensity Factors at Sharp Notches in Elastic Plates," Int. J. Numer. Methods Eng., **20**, pp. 999–1008.
[8] Hong, C. C., and Stern, M., 1978, "The Computation of Stress Intensity Factors in Dissimilar Materials," J. Elast., **8**(1), pp. 21–34.
[9] Carpenter, W. C., and Byers, C., 1987, "A Path Independent Integral for Computing Stress Intensities for V-Notched Cracks in a Bi-Material," Int. J. Fract., **35**, pp. 245–268.
[10] Banks-Sills, L., 1997, "A Conservative Integral for Determining Stress Intensity Factors of a Bimaterial Strip," Int. J. Fract., **86**, pp. 385–398.
[11] Liu, D., and Fleck, N. A., 1999, "Scale Effects in the Initiation of Cracking of a Scarf Joint," Int. J. Fract., **95**, pp. 67–88.
[12] Labossiere, P. E. W., and Dunn, M. L., 1999, "Stress Intensities at Interface Corners in Anisotropic Bimaterials," Eng. Fract. Mech., **62**, pp. 555–575.
[13] Banks-Sills, L., and Sherer, A., 2002, "A Conservative Integral for Determining Stress Intensity Factors of a Bimaterial Notch," Int. J. Fract., **115**, pp. 1–26.
[14] Meda, G., Messner, T. W., Sinclair, G. B., and Solecki, J. S., 1998, "Path-Independent *H* Integrals for Three-Dimensional Fracture Mechanics," Int. J. Fract., **94**, pp. 217–234.
[15] Ortiz, J. E., Mantic, V., and Paris, F., 2006, "A Domain-Independent Integral for Computation Of Stress Intensity Factors Along Three-Dimensional Crack Fronts and Edges by BEM," Int. J. Solids Struct., **43**, pp. 5593–5612.
[16] Hwu, C., Omiya, M., and Kishimoto, K., 2003, "A Key Matrix N for the Stress Singularity of the Anisotropic Elastic Composite Wedges," JSME Int. J., Ser. A, **46**(1), pp. 40–50.
[17] Hwu, C., and Lee, W. J., 2004, "Thermal Effect on the Singular Behavior of Multi-Bonded Anisotropic Wedges," J. Therm. Stresses, **27**(2), pp. 111–136.
[18] Ting, T. C. T., 1996, *Anisotropic Elasticity: Theory and Applications*, Oxford Science Publications, New York.
[19] Hwu, C., and Ikeda, T., 2008, "Electromechanical Fracture Analysis for Corners and Cracks in Piezoelectric Materials," Int. J. Solids Struct., **45**, pp. 5744–5764.
[20] Sokolnikoff, I. S., 1956, *Mathematical Theory of Elasticity*, 2nd ed., McGraw-Hill, New York.
[21] Irwin, G. R., 1962, "Crack-Extension Force for a Part-Through Crack in a Plate," ASME J. Appl. Mech., **29**, pp. 651–654.
[22] Li, S., Mear, M. E., and Xiao, L., 1998, "Symmetric Weak-Form Integral Equation Method for Three-Dimensional Fracture Analysis," Comput. Methods Appl. Mech. Eng., **151**, pp. 435–459.
[23] Sukumar, N., Moes, N., Moran, B., and Belytschko, T., 2000, "Extended Finite Element Method for Three-Dimensional Crack Modelling," Int. J. Numer. Methods Eng., **48**, pp. 1549–1570.
[24] Raju, I. S., and Newmann, J. C., Jr., 1977, "Three-Dimensional Finite Element Analysis of Finite-Thickness Fracture Specimens," NASA Technical Report No. TND-8414.
[25] Kassir, M. K., and Bregman, A. M., 1972, "The Stress Intensity Factor for a Penny-Shaped Crack Between Two Dissimilar Materials," ASME J. Appl. Mech., **39**, pp. 308–310.
[26] Chaudhuri, R. A., 2006, "Three-Dimensional Asymptotic Stress Field in the Vicinity of the Circumference of a Bimaterial Penny-Shaped Interfacial Discontinuity," Int. J. Fract., **141**, pp. 211–225.